Heliyon 10 (2024) e29326

Contents lists available at ScienceDirect

Heliyon

journal homepage: www.cell.com/heliyon

Research article

Identification of N7-methylguanosine-related miRNAs as potential biomarkers for prognosis and drug response in breast cancer

Danian Dai [a,1], Hongkai Zhuang [b,1], Mao Shu [c,1], Lezi Chen [a], Chen Long [d], Hongmei Wu [e,**], Bo Chen [c,*]

[a] Department of Vascular and Plastic Surgery, Guangdong Provincial People's Hospital (Guangdong Academy of Medical Sciences), Southern Medical University, Guangzhou, Guangdong, 510080, China
[b] Department of Hepatobiliary Surgery, Sun Yat-sen Memorial Hospital, Sun Yat-sen University, Guangzhou, 510080, China
[c] Department of Breast Cancer, Cancer Center, Guangdong Provincial People's Hospital (Guangdong Academy of Medical Sciences), Southern Medical University, Guangzhou, 510080, Guangdong, China
[d] Department of Pathology, Yueyang Maternal Child Health-Care Hospital, Yueyang, 414000, Hunan, China
[e] Department of Pathology, Guangdong Provincial People's Hospital (Guangdong Academy of Medical Sciences), Southern Medical University, Guangzhou, China

ARTICLE INFO

Keywords:
N7-methylguanosine
Breast cancer
microRNA
Prognosis
Drug response

ABSTRACT

Objectives: The impact of N7-methylguanosine (m7G) on tumor progression and the regulatory role of microRNAs (miRNAs) in immune function significantly influence breast cancer (BC) prognosis. Investigating the interplay between m7G modification and miRNAs provides novel insights for assessing prognostics and drug responses in BC.

Materials and methods: RNA sequences (miRNA and mRNA profiles) and clinical data for BC were acquired from the Cancer Genome Atlas (TCGA) database. A miRNA signature associated with 15 m7G in this cohort was identified using Cox regression and LASSO. The risk score model was evaluated using Kaplan-Meier and time-dependent ROC analysis, categorizing patients into high-risk and low-risk groups. Functional enrichment analyses were conducted to explore potential pathways. The immune system, including scores, cell infiltration, function, and drug sensitivity, was examined and compared between high-risk and low-risk groups. A nomogram that combines risk scores and clinical factors was developed and validated. Single-sample gene set enrichment analysis (ssGSEA) was employed to explore m7G-related miRNA signatures and immune cell

ABBREVIATION: AUC, Area under the ROC curves; BC, Breast cancer; BP, Biological process; BRCA, Breast invasive carcinoma; CC, Cellular component; CCLE, the Cancer Cell Line Encyclopedia Project; C-index, Concordance index; CTRP, Cancer Therapeutics Response Portal; DEGs, Differentially expressed genes; DEmiRNAs, Differentially expressed miRNAs; DO, Disease Ontology; ER, Estrogen receptor; FC, Fold change; FDR, False discovery rate; GDSC, Data from Sanger's Genomics of Drug Sensitivity; GO, Gene Ontology; IC50, Half-maximal inhibitory concentration; ICIs, Immune checkpoint inhibitors; IPS, Immunophenotype score; KEGG, Kyto Encyclopedia of Genes and Genomes; LASSO, Least absolute shrinkage selection operator; m7G, N7-Methylguanosine; MF, Molecular function; miRNAs, microRNAs; mRNA, Messenger RNA; OS, Overall survival; PR, Progesterone receptor; ROC, Receiver Operating Characteristic; rRNA, Ribosomal RNA; snoRNA, Small nucleolar RNA; snRNA, Small nuclear RNA; ssGSEA, Single-sample gene set enrichment analysis; TCGA, The Cancer Genome Atlas; TCIA, The Cancer Immunome Atlas; TME, Tumor microenvironment; tRNA, Transfer RNA.

* Corresponding author.
** Corresponding author. Department of Pathology, Guangdong Provincial People's Hospital (Guangdong Academy of Medical Sciences), Southern Medical University, Guangzhou, 510080, Guangdong, China.
E-mail addresses: whm-happy@163.com (H. Wu), chenbo@gdph.org.cn (B. Chen).
[1] These authors contributed equally to this work.

https://doi.org/10.1016/j.heliyon.2024.e29326
Received 7 October 2023; Received in revised form 29 March 2024; Accepted 31 March 2024
Available online 6 April 2024

relationships in the tumor microenvironment. Additionally, drug susceptibility was compared between risk groups.

Results: Fifteen m7G-related miRNAs were independently correlated with overall survival (OS) in BC patients. Time-dependent ROC analysis yielded area under the curve (AUC) values of 0.742, 0.726, and 0.712 for predicting 3-, 5-, and 10-year survival rates, respectively. The Kaplan-Meier analysis revealed a significant disparity in OS between the high-risk and low-risk groups ($p = 1.3e-6$). Multiple regression identified the risk score as a significant independent prognostic factor. An excellent calibration nomogram with a C-index of 0.785 (95 % CI: 0.728–0.843) was constructed. In immune analysis, low-risk patients exhibited heightened immune function and increased responsiveness to immunotherapy and chemotherapy compared to high-risk patients.

Conclusion: This study systematically analyzed m7G-related miRNAs and revealed their regulatory mechanisms concerning the tumor microenvironment (TME), pathology, and the prognosis of BC patient. Based on these miRNAs, a prognostic model and nomogram were developed for BC patients, facilitating prognostic assessments. These findings can also assist in predicting treatment responses and guiding medication selection.

1. Introduction

Women are at a heightened risk of developing breast cancer (BC) compared to any other cancer type [1,2]. Over the past two decades, advancements in methods and new medications have significantly increased the 5-year overall survival (OS) rate for early-stage BC patients to over 80 % [3]. Notably, immunotherapy, including PD-1/PD-L1 inhibitors, has shown substantial potential in managing patients with malignant tumors, including BC [4,5]. Some studies, utilizing single-cell technology, are investigating the relationship between breast cancer and the immune microenvironment by analyzing circulating blood components or gene expression [6–8] [6–8] [6–8]. The objective is to discover breakthroughs in the field of tumor immunotherapy. Nevertheless, despite these commendable advancements, certain patients face unfavorable prognoses due to drug resistance, metastasis, and recurrence [9]. Consequently, there is an urgent need to identify novel and distinct predictive markers that could aid in classifying patients based on prognosis and tailoring personalized treatments.

RNA epigenetic modifications play crucial roles in various biological processes, with over 100 identified RNA-modified nucleosides to date [10,11]. Several types of base modifications are used to regulate messenger RNA (mRNA), including N7-Methylguanosine (m7G) as an epigenetic modification [12]. Besides mRNA, m7G also occurs in transfer RNA (tRNA), ribosomal RNA (rRNA), small nucleolar RNA (snoRNA), microRNA (miRNA), and small nuclear RNA (snRNA) [13]. A growing body of evidence suggests that m7G plays a pivotal role in cancer development and progression by modulating various oncogenes and tumor suppressor genes [14]. Reports indicate that METTL1/WDR4-related m7G modification enhances the expression of cell cycle progression genes by reshaping mRNA translation activity, contributing to the development of acute myeloid leukemia [15]. In a study of head and neck tumor, higher infiltration of $CD4^+$ T cells and $CD8^+$ T cells was observed in the tumor microenvironment in METTL1 knockout mice, with lower infiltration of Tregs and Th17 cells [16]. Tumor immunotherapy may also depend on m7G, according to this result. Despite some existing research on m7G, further investigation is required to understand the relationship between m7G and the tumor microenvironment (TME) more comprehensively. A thorough analysis of this relationship will enhance our understanding of m7G-mediated cellular infiltration in the BC TME and unveil potential mechanisms that increase BC prognosis, offering new ideas for precision therapy.

Noncoding miRNAs (about 22 nucleotides long) are responsible for silencing RNA and regulating gene expression post-transcription. The distinct miRNA expression patterns observed in cancer represents a valuable resource for sensitive biomarker identification in cancer risk assessment, outcome prognosis, and the categorization of histological subtypes [17]. Simultaneously , miRNAs also play a significant role in regulating drug sensitivity and predicting drug response in BC. Previous studies have demonstrated that the methyltransferase METTL1 mediates m7G modification of specific miRNAs, promoting their maturation and inhibiting lung cancer cell migration [18]. Xie et al. identified the METTL1/m7G/miR-760/ATF3 axis as a regulator of bladder cancer progression and presented potential therapeutic targets for treating bladder cancer [19]. Therefore, further exploration of the functional and regulatory network involving m7G modification and miRNAs in BC will contribute to novel approaches for prognostic assessments or drug response predictions in BC.

In this study, we developed a miRNA prognostic model utilizing m7G and constructed a nomogram for BC patients to assess their prognosis. Leveraging the m7G-related miRNA signature, we conducted comprehensive analyses of the TME, immune cell infiltration, immune function, and drug sensitivity using pertinent publicly available data. This approach holds the potential to improve the prediction and prognosis of BC patients while identifying potential therapeutic targets.

2. Materials and methods

2.1. Data collection and processing for breast cancer

The Cancer Genome Atlas (TCGA) database, available at https://portal.gdc.cancer.gov, housed comprehensive RNA sequencing data and clinical records about BC. The miRNA sequencing data (Isoform Expression) encompassed 1103 BC samples and 104 samples

from healthy breast tissue. The mRNA sequencing data (TCGA-BRCA, HTSeq-FPKM) comprised 1104 BC samples and 114 healthy samples. Statistical analysis was conducted without patients who had incomplete data or had not been followed up for 30 days. In the next step, 1026 BC samples were analyzed clinically.

2.2. Identification of m7G-Related genes and differentially expressed miRNAs in BC

According to previous studies [20,21], 44 genes related to m7G were identified. We predicted a total of 5761 miRNAs that target these m7G-related genes using the TargetScan database, accessible at http://www.targetscan.org. We used the R package "limma" to evaluate the expression of 5761 miRNAs associated with m7G in the TCGA BC cohorts and normal samples. Then, we screened the miRNAs with the standard of $|\log2FC| > 1.5$, FDR <0.05, and eventually, 204 m7G-related differentially expressed miRNAs (DEmiRNAs) were selected. The volcano plot and heatmap illustrate the expression of m7G-related DEmiRNAs.

2.3. Construction and validation of prognostic signature

We also conducted a univariate Cox regression analysis to investigate whether the 204 m7G-related DEmiRNAs were linked to survival in the TCGA dataset. We selected candidate prognostic miRNAs through the LASSO regression model (utilizing the R package "glmnet") based on univariate analysis with p-values below 0.05. A risk score was established for each miRNA identified in the LASSO analysis based on multivariate Cox regression analysis. The forest plot of prognostic miRNAs was drawn by a "forestplot" R package. Based on the identified DEmiRNAs, the subsequent equation was employed for determining the risk assessment:

$$\text{Risk score} = \sum_{i=1}^{n} \text{Coefi} * \text{Expi},$$

In LASSO regression, N represents the number of selected miRNAs, Coefi stands for the regression coefficient, and Expi represents the expression value of each miRNA. Patients from the TCGA BRCA dataset were categorized into low and high risk groups using the median risk score as the threshold, and we compared the two risk groups using Kaplan-Meier survival estimates. We also estimated sensitivity and specificity for survival at 3-, 5-, and 10-year intervals using time-dependent ROC curves and area under the ROC curves (AUC).

2.4. Construction and validation of nomogram

A nomogram was constructed using the packages "survival", "survminer", "regplot" and "rms" in R. To assess the prognostic value of the risk score signature and traditional clinical factors (including age, stage, T, N, progestogen receptor (PR) status, estrogen receptor (ER) status, and HER2 receptor status), univariate and multivariate Cox regression analyses were conducted. A nomogram was constructed to forecast survival probabilities over 3-, 5-, and 10-year periods based on the clinicopathologic features and m7G-related risk score. To evaluate the accuracy of the modelling method, the AUC value was calculated. Subsequently, calibration plots measured the nomogram's discriminant capacity using the concordance index (C-index).

2.5. Functional enrichment analysis

We identified differentially expressed genes (DEGs) between the high-risk and low-risk groups utilizing the R packages "limma" and "edgeR" applying the following criteria: $|\log2\text{Fold Change (FC)}| > 0.5$ and False discovery rate (FDR) < 0.05. ESTIMATE (Estimation of Stromal Cells and Immune Cells in Malignant Tumor Tissues), a bioinformatics algorithm, was used to quantitate each BRCA patient's TME score (https://bioinformatics.mdanderson.org) [22]. BRCA patients were divided into two groups, high immunoscore and low immunoscore, based on their immunoscore within the TME. We obtained immune-related genes that were differentially expressed using the following criteria: $|\log2FC| > 1$ and FDR <0.05. We identified immune-related genes associated with risk through an intersection with immune-risk genes. To reveal the biological processes and potential signaling pathways associated with diseases, we performed Gene Ontology (GO), Kyoto Encyclopedia of Genes and Genomes (KEGG), and Disease Ontology (DO) analyses. The analyses were conducted using R packages such as "org.Hs.eg.db", "clusterProfiler", and "enrichplot" [23,24].

2.6. Immune analysis

Utilizing single-sample gene set enrichment analysis (ssGSEA), we quantified 29 immune signatures, including 13 functions related to the immune system and 16 distinct immune cell types. We initially employed the Pearson coefficient test to assess the internal correlations among various immune characteristics, followed by the Wilcoxon test to determine disparities in both immune cells and functions between the two groups. Lastly, we examined the expression levels of 32 immune checkpoint-related genes in the two risk groups to anticipate the potential efficacy of immune checkpoint blockade therapy.

2.7. Immunotherapy sensitivity analysis

Immunotherapy susceptibility data were downloaded from The Cancer Immunome Atlas (TCIA, https://tcia.at/home) [25,26].

TCIA contains a comprehensive immunogenomic analysis of RNA-seq data from 20 solid cancers. The immunophenotype score (IPS) refers to the assessment of effector cells, immunosuppressive cells, MHC molecules, and immunomodulators that determine immunogenicity and is based on unbiased gene expression in representative cell types using machine learning methods, calculated within a range of 0–10 for the IPS. IPS results for BC patients were downloaded from the TCIA database. This study utilized data from the TCGA-BRCA cohort to discover the association between immunotherapy sensitivity and risk grouping of m7G-related miRNAs.

2.8. *OncoPredict for drug sensitivity analysis*

Maeser and colleagues created the R package "oncoppredict" to forecast drug responsiveness in cancer individuals [27]. We utilized the "calcPhenotype" function within the "oncoppredict" R package to compute the half-maximal inhibitory concentrations (IC50) for tumor cell lines, leveraging the tissue's gene expression profile to predict sensitivity to the chemotherapy drugs. Data on cancer drug sensitivity from Sanger's Genomics of Drug Sensitivity in Cancer (GDSC; http://www.cancerrxgene.org/en/) and the Broad Institute's

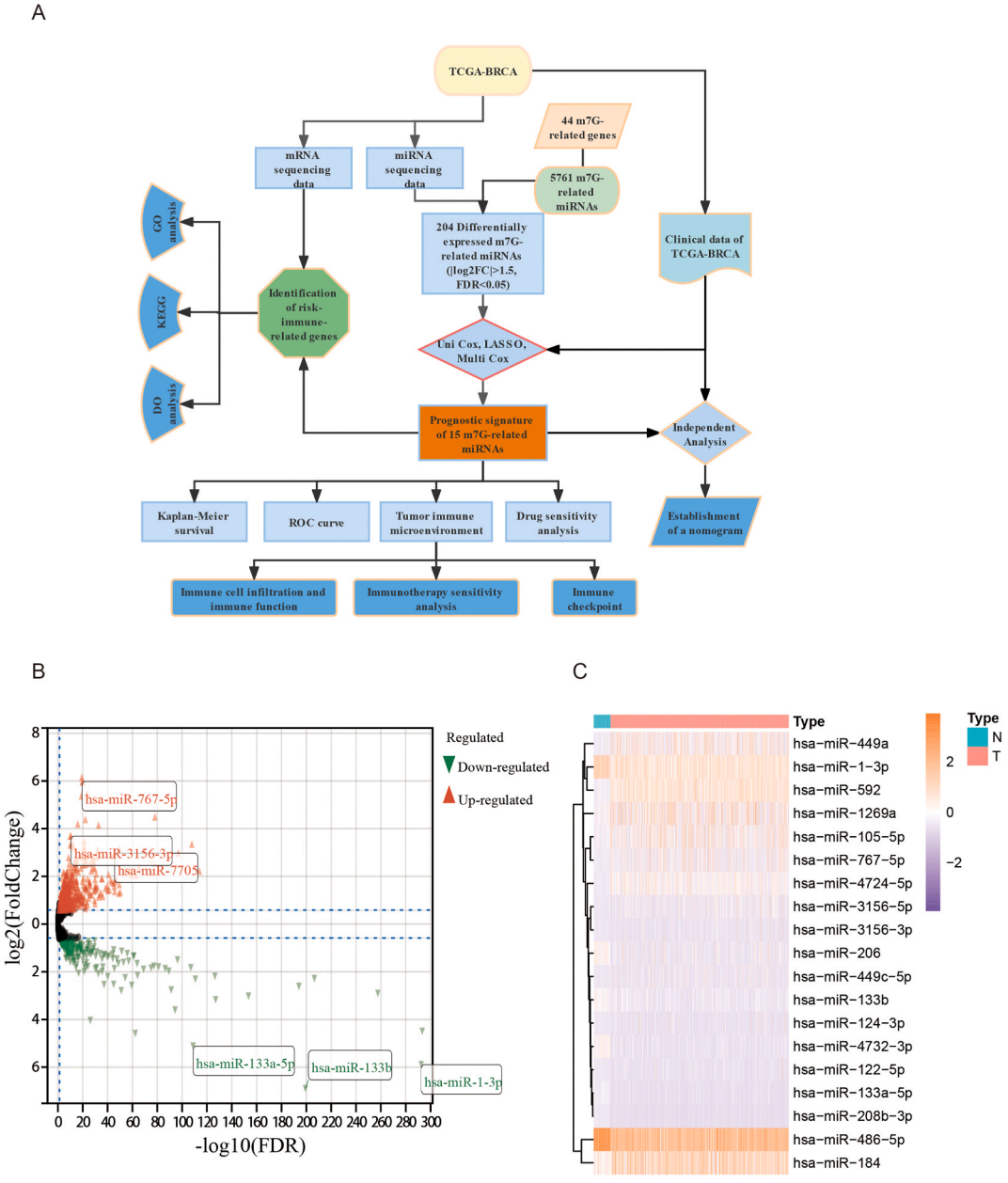

Fig. 1. DEmiRNAs targeting m7G-related genes (A) A flow chart of the study. (B) The volcano plot of 204 DEmiRNAs. (C) A heatmap of the top 20 DEmiRNAs between normal (N) and tumor (T) breast samples. DEmiRNAs, Differentially expressed miRNAs.

Cancer Therapeutics Response Portal (CTRP) were incorporated into the "oncoppredict" R package as training datasets. Gene expression profiles of cell lines, used to predict drug responses, were sourced from the Cancer Cell Line Encyclopedia project (CCLE; http://portals.broadinstitute.org/ccle). Our study encompassed a total of 198 drugs, and we employed an unpaired *t*-test to assess drug sensitivity between the high- and low-risk groups, with a significance threshold set at $P < 0.05$.

2.9. Statistical analysis

We conducted an analysis of miRNA and mRNA expression levels, contrasting tumor samples with neighboring non-cancerous samples using Student's t-test. Additionally, we utilized Pearson's chi-square test to compare categorical variables. To assess patient survival, we employed the Kaplan-Meier analysis and the two-sided log-rank test to compare survival curves. We applied both single-variable and multiple-variable Cox regression models to evaluate independent prognostic models. Both groups underwent comparison using the Mann-Whitney test for both filtration and immune pathway activation. Statistical analysis was performed using R software (v4.2.1). Some of the images in this study were generated using the Sangerbox online drawing tool (http://www.sangerbox.com/tool) [28]. We considered a P-value less than 0.05 from both sides to indicate statistical significance.

3. Results

3.1. m7G-related miRNAs and their expression levels

The study process flowchart is depicted in Fig. 1A. We selected 44 m7G-related genes based on previously documented literature

Table 1
Characteristics of TCGA-BRCA patients.

Characteristics	BRCA cohort	Percentage(%)
Total number of patients	1026	100.0
Age (median, range),year	58(26–89)	
Sex		
Female	1014	98.8
Male	12	1.2
Survival time		
OS days (median, range)	894.5(30–8605)	
Stage		
I	180	17.5
II	577	56.2
III	228	22.2
IV	19	1.9
Unknown	22	2.1
T		
T1	277	27.0
T2	583	56.8
T3	127	12.4
T4	36	3.5
Unknown	3	0.3
N		
N0	479	46.7
N1+N2+N3	530	51.7
Unknown	17	1.7
M		
M0	848	82.7
M1	20	1.9
Unknown	158	15.4
PR status		
Negative	312	30.4
Positive	669	65.2
Unknown	45	4.4
ER status		
Negative	219	21.3
Positive	764	74.5
Unknown	43	4.2
HER2 status		
Negative	526	51.3
Positive	147	14.3
Equivocal	187	18.2
Unknown	166	16.2

Abbreviation: TCGA, the Cancer Genome Atlas; BRCA, Breast invasive carcinoma; OS, Overall survival; T, Tumor; N, Lymph nodes; M, Metastasis; PR, Progesterone receptor; ER, Estrogen receptor; HER2, Human epidermal growth factor receptor 2.

sources (Supplementary Table S1) and retrieved 5761 m7G-related miRNAs from the TargetScan database (Supplementary Table S2). A total of 1207 breast samples with miRNA sequencing data from The Cancer Genome Atlas (TCGA) were included, comprising 1103 tumor tissues and 104 normal tissues. Furthermore, we identified 204 differentially expressed miRNAs (DEmiRNAs) related to m7G (|log2FC|>1.5 and FDR <0.05), with 151 upregulated and 53 downregulated DEmiRNAs (Fig. 1B). The heatmap illustrates the expression of the top 20 m7G-related DEmiRNAs (Fig. 1C).

3.2. miRNA signatures related to m7G constructed and validated

Considering samples with incomplete clinical data, a total of 1026 samples were analyzed (Table 1). Initially, 204 DEmiRNAs were screened using univariate Cox regression analysis. To maintain the prognostic value of the final model, a cutoff value of $p < 0.05$ was

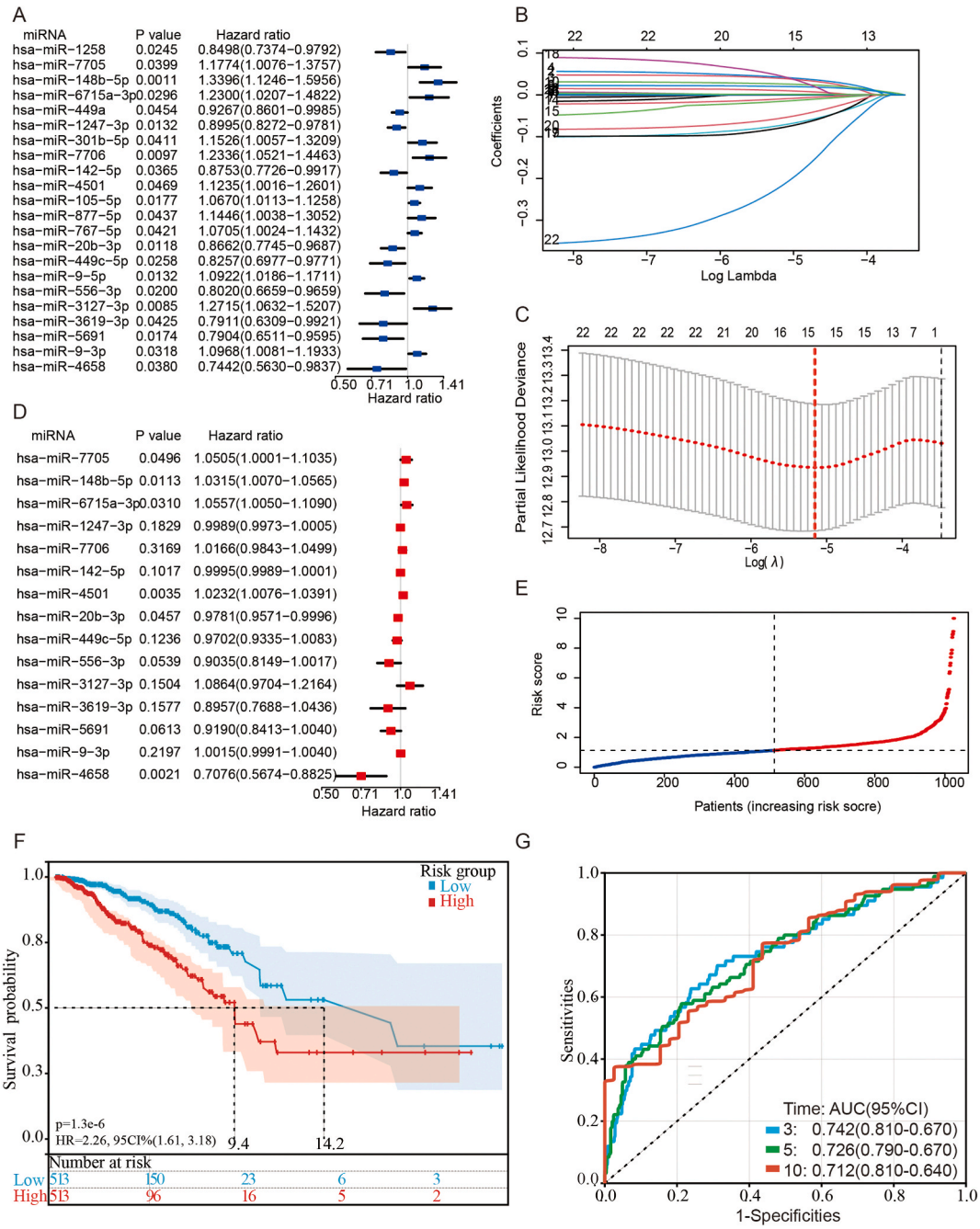

Fig. 2. Construction of a novel m7G-related miRNA risk signature and its prognostic value.

set, resulting in 22 miRNAs with prognostic significance (Fig. 2A). Further screening through Cox regression analysis yielded 15 miRNA combinations with the optimal λ value (Fig. 2B and C). These 15 miRNAs correspondingly regulate four m7G-related genes, including AGO2, CCNB1, DCP2 and CYFIP1 (Supplementary Table S3). Multivariate Cox regression on 15 miRNAs revealed that miR-7705 (p = 0.0496), miR-148b-5p (p = 0.0113), miR-6715a-3p (p = 0.0310), and miR-4501 (p = 0.0035) may act as risk factors; while

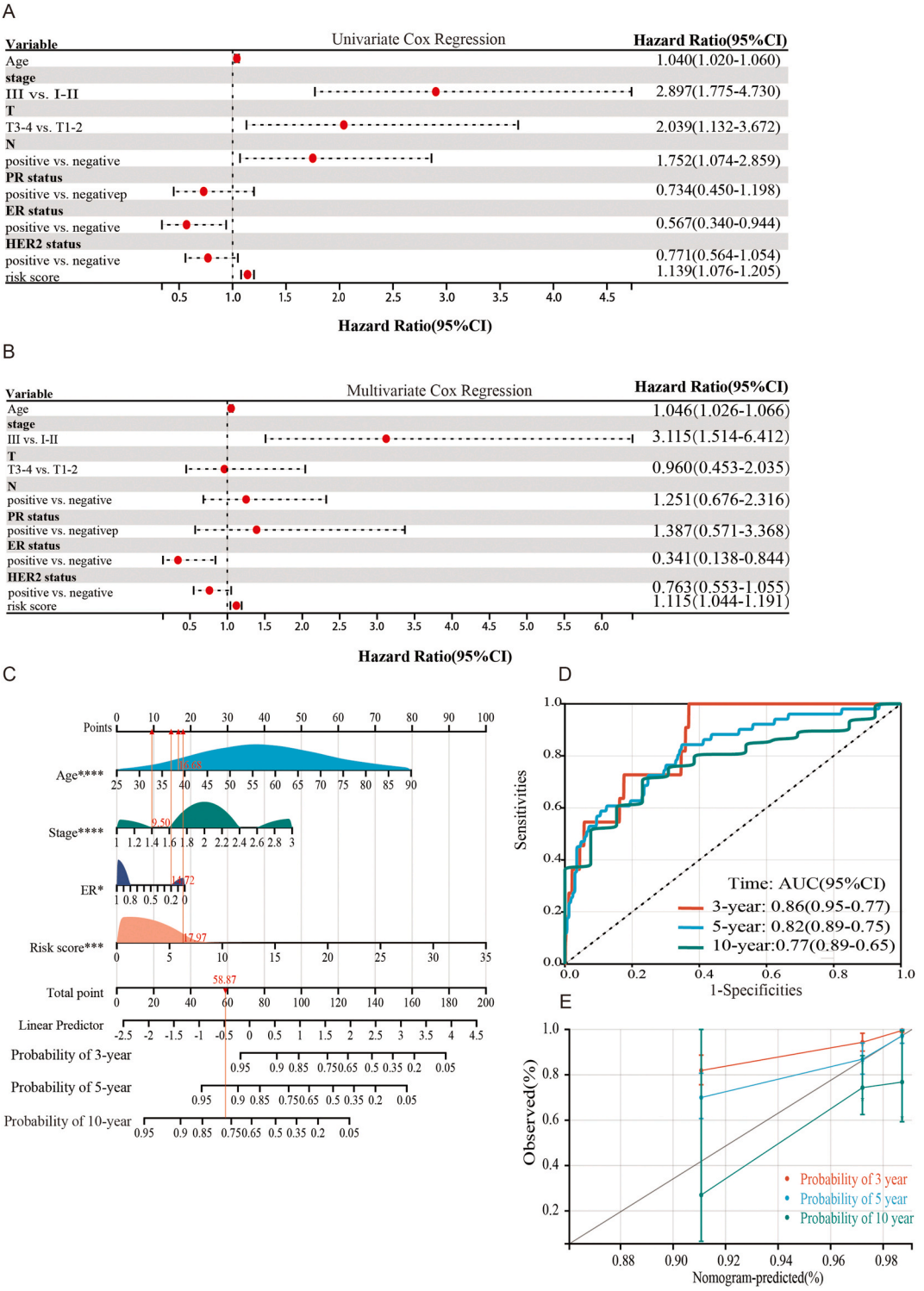

Fig. 3. Development and assessment of Nomogram.

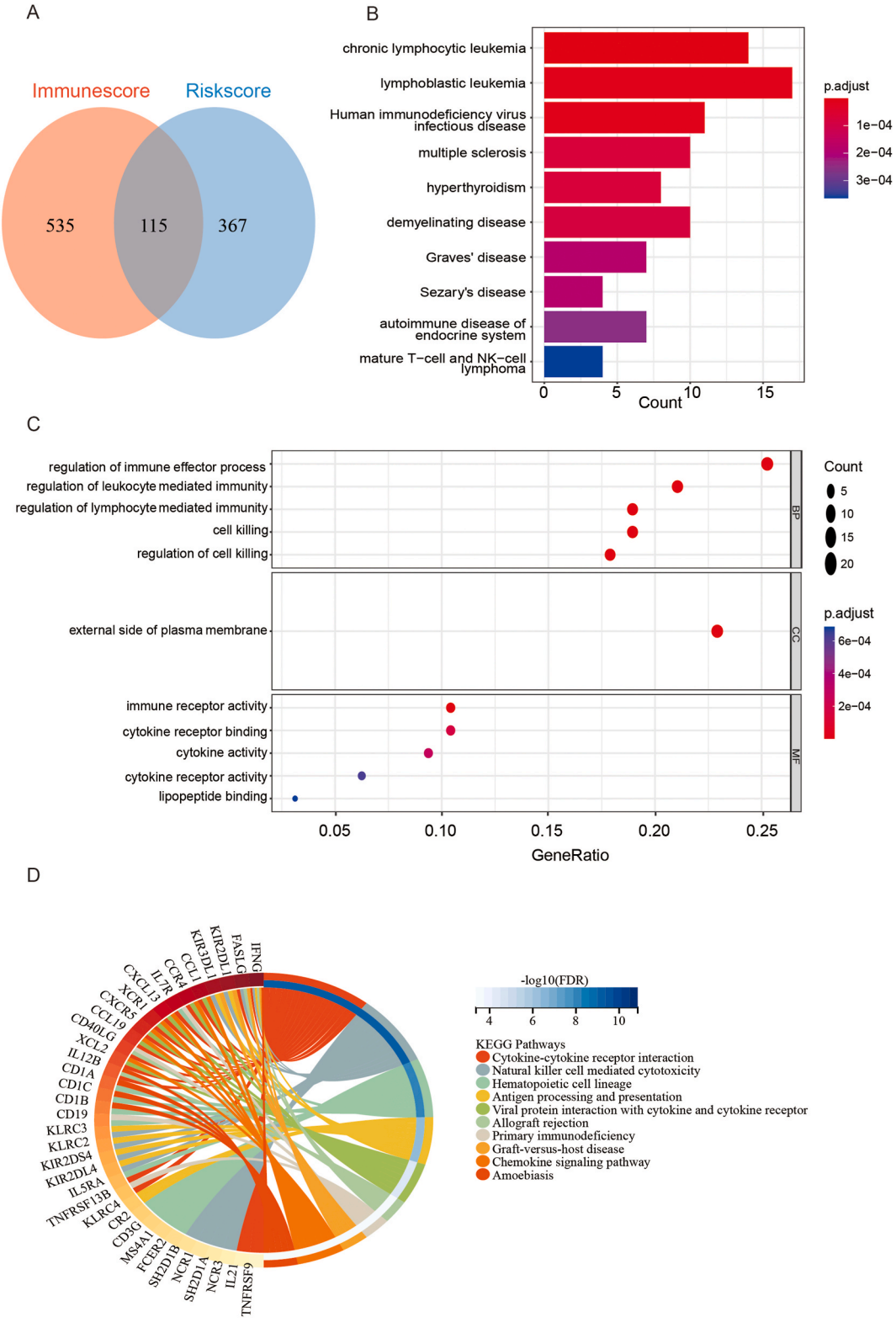

Fig. 4. Functional analysis based on the Intersection of genes.

miR-20b-3p (p = 0.0457) and miR-4658 (p = 0.0021) may function as protective factors (Fig. 2D). To compute the risk scores for BC patients, the following formula was employed: Riskscore=(0.0393*miR-7705 expression)+(0.0262*miR-148b-5p)+(0.0423*miR-6715a-3p)+(−0.0006*miR-1247-3p)+(0.0103*miR-7706)+(−0.0004*miR-142-5p)+(0.0202*miR-4501)+(−0.0097*miR-20b-3p)+(−0.0153*miR-449c-5p)+(−0.0724*miR-556-3p)+(0.0446*miR-3127-3p)+(−0.0783*miR-3619-3p)+(−0.0553*miR-5691)+(0.0014*miR-9-3p)+(−0.2170*miR-4658). Patients were categorized into high-risk and low-risk groups based on the median risk scores (Fig. 2E). A Kaplan-Meier analysis examined the association between risk signatures and prognosis, revealing survival differences between high-risk and low-risk groups of BC patients. The median OS of the low-risk group was nearly five months longer than that of the high-risk group (Fig. 2F). The sensitivity and specificity of prognostic signatures of m7G-related miRNAs were assessed by time-dependent ROC analysis, revealing area under the curve (AUC) values of approximately 0.742 for 3-year, 0.726 for 5-year, and 0.712 for 10-year (Fig. 2G).

(A) A Cox univariate analysis identified 22 prognostic miRNAs related to m7G. (B) An analysis of 22 prognostic miRNAs related to m7G using LASSO. (C) In the TCGA BRCA cohort, 22 miRNA signatures were identified and evaluated using the Lasso algorithm, and 15 miRNAs were screened for developing patient prognosis risk signatures. The red line shows the final number of miRNAs selected. (D) Based on the multivariate Cox regression analysis, the forest plot illustrates the independent prognostic value of the 15 miRNAs. (F) In the Kaplan-Meier method, the overall survival rate of BC patients was compared between high-risk and low-risk groups. (G) A time-dependent ROC curve for predicting OS based on the m7G-related miRNA risk score. LASSO, Least absolute shrinkage selection operator; TCGA, The Cancer Genome Atlas; BRCA, Breast invasive carcinoma; ROC, Receiver operating characteristic; OS, Overall survival.

3.3. Nomogram construction and verification

To evaluate the potential of the risk score as an independent prognostic indicator, both univariate and multivariate Cox regression analyses were conducted, incorporating clinical factors (such as age, stage, T, N, progesterone receptor (PR) status, estrogen receptor (ER) status, and HER2 status) along with the risk scores. Univariate analysis showed that age (HR = 1.040, 95%CI[1.020–1.060]), stage (HR = 2.897, 95%CI[1.775–4.730]), T (HR = 2.039, 95%CI[1.132–3.672]), N (HR = 1.752, 95%CI[1.074–2.859]), ER (HR = 0.567, 95%CI[0.340–0.944]), and risk score (HR = 1.139, 95%CI[1.076–1.205]) were associated with OS in BC patients (Fig. 3A). However, following multivariate Cox analysis (Fig. 3B), only age (HR = 1.046, 95 % CI [1.026–1.066]), stage (HR = 3.115, 95 % CI [1.514–6.412]), ER status (HR = 0.341, 95 % CI [0.138–0.844]), and risk score (HR = 1.115, 95 % CI [1.044–1.191]) retained their status as independent factors for OS. Combining all independent prognostic factors, we constructed a nomogram for predicting 3-, 5-, and 10-year OS rates for all BC patients (Fig. 3C). The C-index of the nomogram model is 0.785 (95 % CI [0.728–0.842]), indicating good discriminative performance. Additionally, the time-dependent AUCs for 3-, 5-, and 10-year intervals were 0.86 (95 % CI [0.77–0.95]), 0.82 (95 % CI [0.75–0.89]), and 0.77 (95 % CI [0.65–0.89]), respectively, demonstrating strong predictive performance (Fig. 3D). Calibration curves illustrated the nomogram's high discriminative ability (Fig. 3E). Overall, the nomogram model accurately predicted OS for BC patients.

(A and B) Forest plots show the prognostic value of Uni-Cox and multi-Cox regression analysis combined with clinical and risk score factors. (C) Combined with age, stage, ER and risk score, a nomogram was established to quantitatively predict the 3-, 5- and 10-year survival of BC patients. *p < 0.05, **p < 0.01, ***p < 0.001, ****P < 0.0001. (D) The time-dependent ROC curves for prognosis of 3-, 5-, and 10-year. (E) Nomogram calibration curves of OS prediction at 3-, 5-, and 10-year for BC patients. ER, Estrogen receptor; ROC, Receiver operating characteristic; OS, Overall survival.

3.4. Functional analysis within the BRCA cohort utilizing risk score and immune score

To elucidate the biological functions and pathways associated with both the immune score and risk score, we initially identified the overlap between the 482 risk-related differentially expressed genes (DEGs) in the risk groups and the 650 immune-related DEGs in the immune groups, resulting in the identification of 115 risk-immune-related genes (Fig. 4A and Supplementary Table S4). A functional analysis of these risk-immune-related genes was then conducted using DO analysis, GO enrichment, and KEGG pathways. The top five relevant terms in the DO analysis were chronic lymphocytic leukemia, lymphocytic leukemia, human immunodeficiency virus infectious disease, multiple sclerosis, and hyperthyroidism (Fig. 4B). The GO enrichment encompassed biological processes (BP), cellular components (CC), and molecular functions (MF). The intersecting genes were significantly enriched in processes such as the regulation of immune effector process, external side of the plasma membrane, and immune receptor activity (Fig. 4C). The KEGG analysis indicated that these genes were associated with various immune pathways, including cytokine-cytokine receptor interaction, natural killer cell-mediated cytotoxicity, and antigen processing and presentation, among others (Fig. 4D).

(A) Venn plot of the intersection genes in both risk score and immune score. (B) Top 10 crucial terms for DO analysis. (C) Top 5 critical terms for GO functional enrichment, including biological process (BP), cellular components (CC), and molecular functions (MF). (D) The circle diagram is enriched in the KEGG analysis. DO, Disease ontology; GO, Gene ontology; KEGG, Kyto encyclopedia of genes and genomes; BP, Biological process; CC, Cellular component; MF, Molecular function.

3.5. The relationship between m7G-related risk signature and immune microenvironment

Considering the close relationship between immunotherapy efficacy and the tumor microenvironment (TME), we further enriched scores for 16 immune cell subsets and 13 immune functions in the TCGA-BRCA cohort using single-sample gene set enrichment analysis

(ssGSEA) (Fig. 5A). A correlation analysis of immune cells revealed a strong positive relationship between tumor-infiltrating lymphocytes (TIL) and $CD8^+$ T cells (r = 0.89), as well as pCDs (r = 0.87) (Fig. 5B). Regarding immune functions, T cell co-inhibition and checkpoint exhibited the highest positive correlation (r = 0.96), while the remaining immune functions showing notably strong

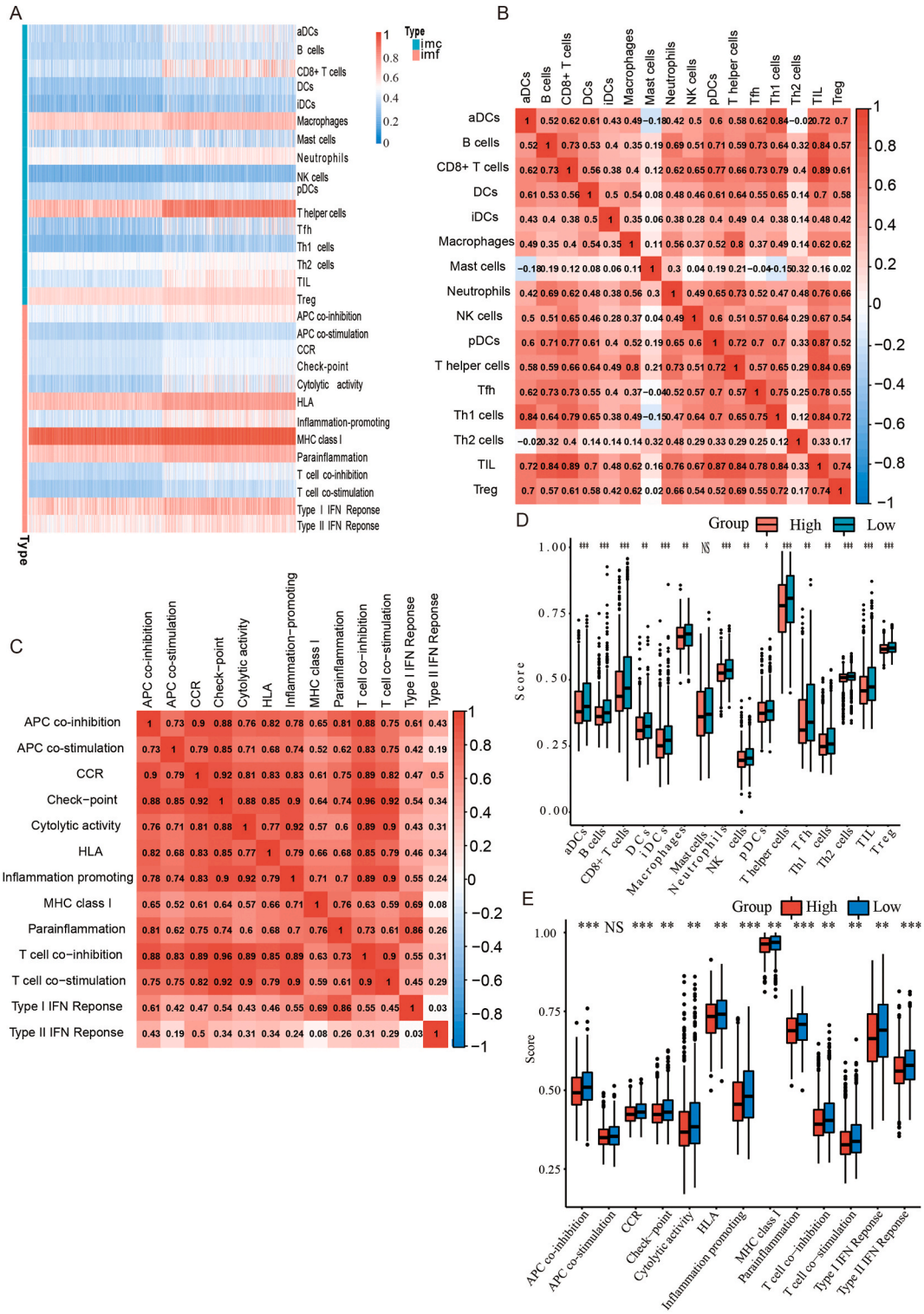

Fig. 5. The ssGSEA analyses of immune cells and immune-related pathways.

positive correlations (Fig. 5C). Subsequently, we assessed the differences in the immune profile differences between the high-risk and low-risk cohorts. Except for mast cells, the presence of other immune cells was notably reduced in high-risk patients (Fig. 5D). Similarly, compared to the low-risk group, all immune functions in the high-risk group, except for APC co-stimulation, exhibited significant down-regulation (Fig. 5E). Therefore, miRNAs related to m7G show promise in predicting immune responses.

(A) The heatmap shows the infiltration of 16 immune cells and 13 immune-related pathways. (B) Correlation between immune cells (the redder the color, the higher the correlation). (C) Correlation between immune-related pathways (the redder the color, the higher the correlation). (D) The boxplot for 16 types of immune cells between the high- and low-risk groups. (E) The boxplot for 13 immune-related pathways between the high- and low-risk groups. P values were showed as: *P < 0.05; **P < 0.01; ***P < 0.001; NS, not significant.

3.6. Expression levels of immune checkpoints and prediction of immune efficacy

As immune cell infiltration abundance correlates with immune checkpoint gene expression levels, we further examined the expression levels of 32 immune checkpoint genes between high and low-risk groups. In the TCGA-BRCA cohort, 30 ICGs (including CTLA-4 and PDCD1) were significantly overexpressed in the low-risk group compared with the high-risk group, except for ICOSSLG and CD276 gene expression levels. Given that CTLA-4 and PD-1 inhibitors are commonly used in BC immunotherapy, we selected these two immune checkpoints as representatives to evaluate the therapeutic effect of immune checkpoint inhibitors (ICIs) through the IPS. When evaluating Immune Prognostic Scores (IPS), which included CTLA4- PD1-, CTLA4- PD1+, CTLA4+ PD1-, and CTLA4+ PD1+,

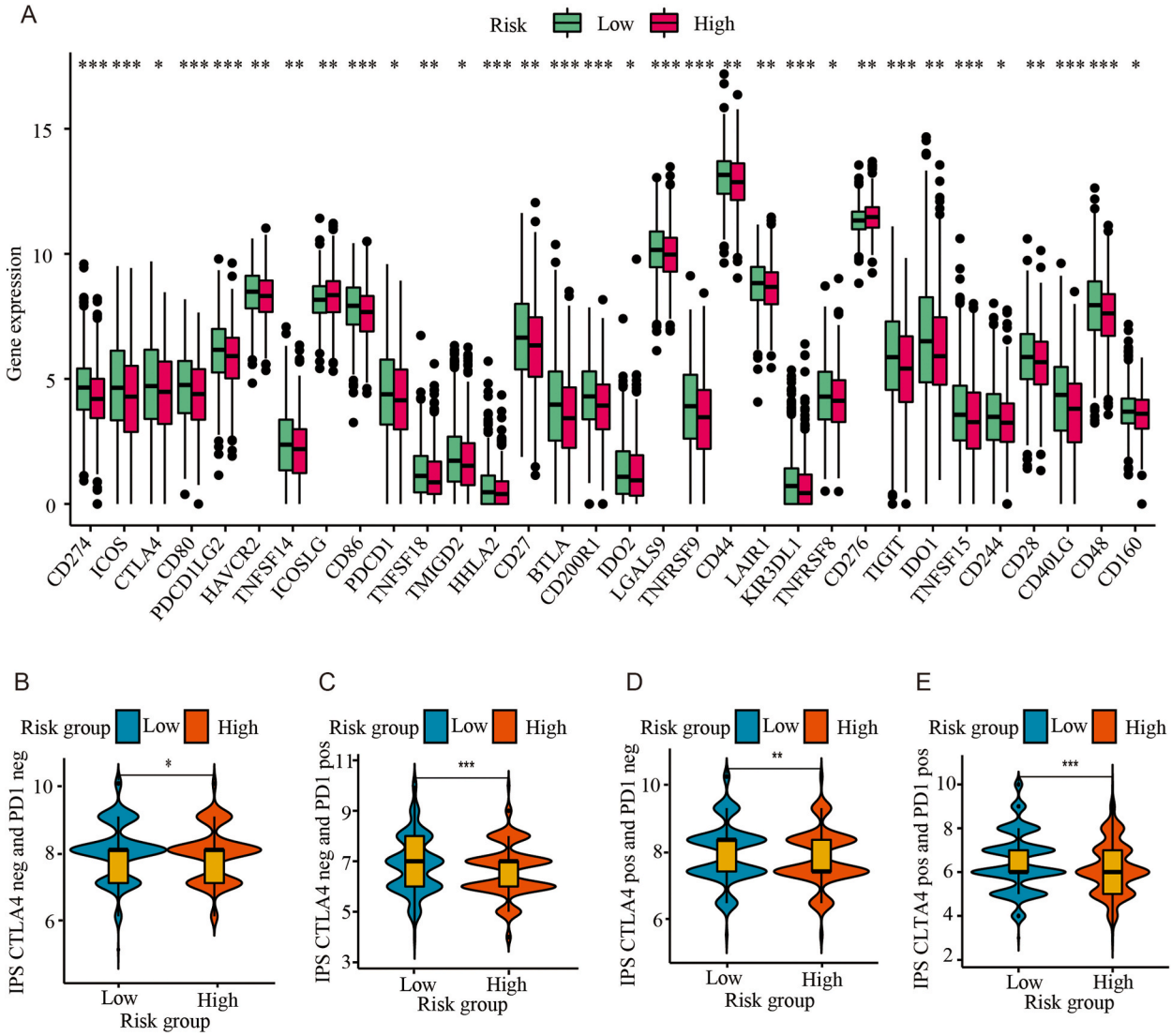

Fig. 6. Immune checkpoint related genes expression and immunotherapy prediction in two risk groups.

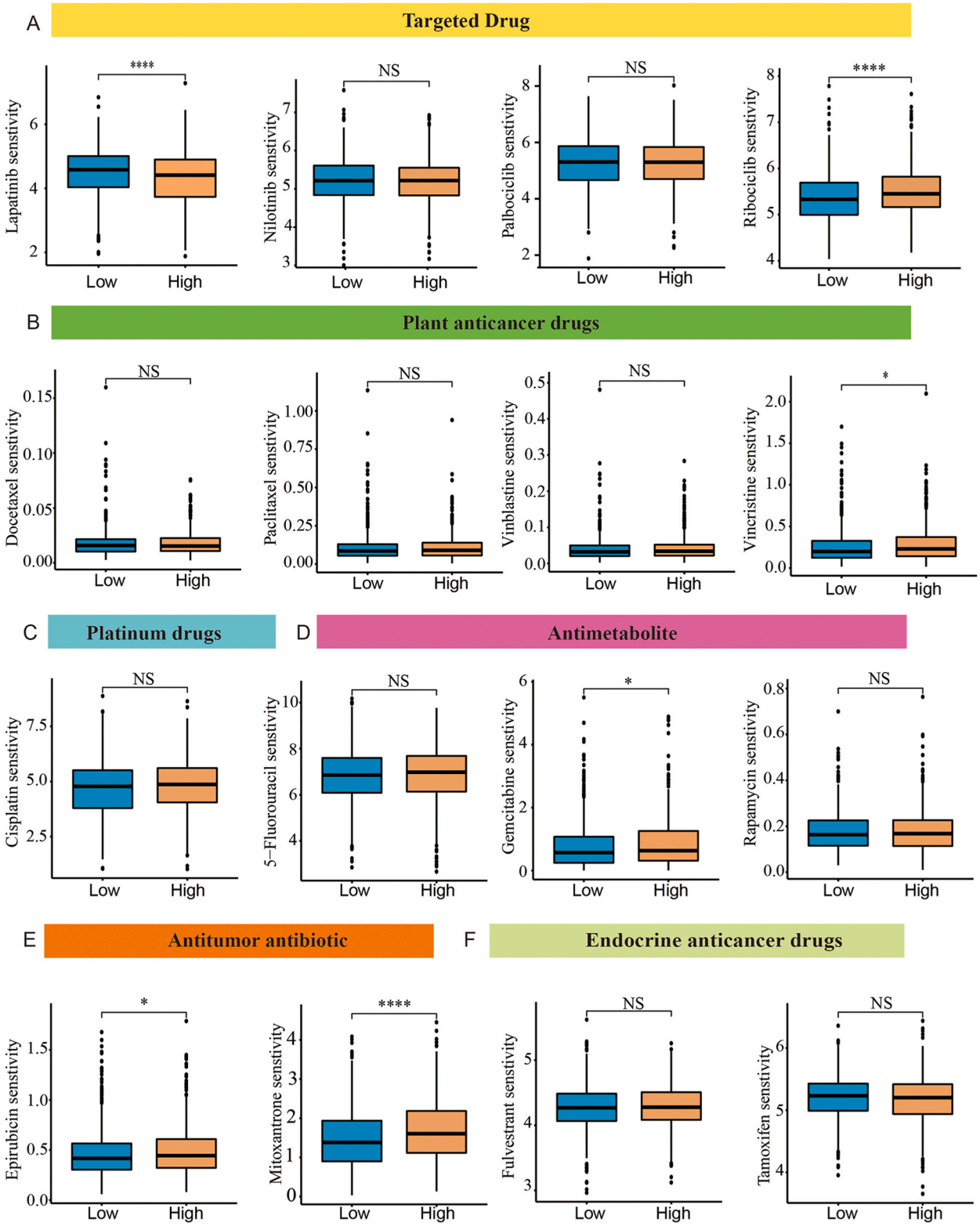

Fig. 7. Chemotherapy drug sensitivity assessment in two risk groups.

across various risk groups, using data from the TICA website, we observed that in all of these condition types, the low-risk group displayed significantly higher IPS (Fig. 6B–E, all $p < 0.05$). These results indicate that individuals classified as low-risk may exhibit heightened responsiveness to ICIs treatment.

(A) Expression of 32 immune checkpoint-related genes in both groups. Responsiveness to CTLA-4 and PD-1 therapy based on TCIA database. (B) Violin plot of IPS scores in Negative CTLA-4 and Negative PD-1. (C) Violin plot of IPS scores in Negative CTLA-4 and Positive PD-1. (D) Violin plot of IPS scores in Positive CTLA-4 and Negative PD-1. (E) Violin plot of IPS scores in Positive CTLA-4 and Positive PD-1. P values were showed as: *$P < 0.05$; **$P < 0.01$; ***$P < 0.001$; NS, not significant. TCIA, The Cancer Immunome Atlas; IPS, Immunophenoscore.

3.7. Comparison of susceptibility to chemotherapeutic drugs among risk groups

To fortify the connection between m7G-related miRNA signatures and clinical applications, we utilized the "oncoPredict" package to predict drug sensitivities for 16 commonly used drugs in BC patients. The findings indicated that the low-risk group exhibited enhanced sensitivity to ribociclib among targeted drugs, vincristine in plant-based anticancer drugs, gemcitabine in anti-metabolites, as well as epirubicin and mitoxantrone within the category of anti-tumor antibiotics. Conversely, the high-risk group demonstrated increased sensitivity to lapatinib (Fig. 7A–E). However, the sensitivity of the two risk groups to other targeted drugs (nilotinib and palbociclib), plant anticancer drugs (docetaxel, paclitaxel, and vinblastine), cisplatin, antimetabolite (5-fluorouracil, and rapamycin) and endocrine anticancer drugs (tamoxifen and fulvestrant) showed no statistically significant difference.

(A) Sensitivity assessment of targeted drugs by lapatinib, nilotinib, palbociclib, and ribociclib, respectively. (B) Sensitivity assessment of plant aiticancer drugs by docetaxel, paclitaxel, vinblastine, and vincristine, respectively. (C) Sensitivity assessment of platinum drug by cisplatin. (D) Sensitivity assessment of antimetabolic anticarcinoma drug by 5-fluorouracil, gemcitabine, and rapamycin. (E) Sensitivity assessment of antitumor antibiotic drugs by epirubicin and mitoxantrone, respectively. (F) Sensitivity assessment of hormonal anticancer drugs of fulvestrant and tamoxifen, respectively. A smaller value for drug sensitivity indicated that the tumor was predicted to be more sensitive to that drug. P values were showed as: *$P < 0.05$; **$P < 0.01$; ***$P < 0.001$; NS, not significant.

4. Discussion

In the era of precision medicine, the quest for a more precise method to assess the prognosis of BC patients and guide treatment is an urgent and essential topic. The epigenetic and immune microenvironment factors play critical roles in BC's tumorigenesis, progression, and drug sensitivity [29,30]. Increasingly, more and more studies have revealed the close relationship between the TME and immune-related features with tumor prognoses. For instance, the degree of tumor infiltration by immune cells has been identified as a predictor of early recurrence and patient prognosis [31]. Additionally, m7G-related METTL1 has been found to regulate the accumulation of polymorphonuclear myeloid-derived suppressor cells in the TME and influence the efficacy of *anti*-PD-1 therapy [32]. However, there is a scarcity of studies constructing BC prognosis models based on m7G-related miRNAs and systematically analyzing the TME and immunotherapy.

Numerous studies have confirmed that miRNAs can regulate a wide range of oncogenes and tumor suppressor genes, with their expression patterns integrated into clinical practice as diagnostic and prognostic indicators [33]. Afterwards, 204 DEmiRNAs between normal breast tissue and BC tissue were analyzed by TCGA database, of which 22 DEmiRNAs had prognostic value. Further, the risk signature, including 15 miRNAs, was obtained by LASS-COX regression analysis. Interestingly, 12 out of the 15 miRNAs primarily regulated m7G-related genes with AGO2 being a prominent target (Supplementary Table S3). AGO2, a translation protein, inhibits mRNA translation by binding to the m7G cap of mRNA targets [34]. The enriched LncRNA CCAT1, for instance, can negatively regulate miR-148b expression through the AGO complex, thereby reducing the radiosensitivity of BC [35]. Except for miR-6715a, miR-3127-3p and miR-4658, other miR-1247-3p [36], miR-142-5p [37], miR-20b-3p [38], miR-449c-5p [39], miR-556-3p [40], miR-3619-3p [41], miR-5691 [42], miR-9-3p [43] also have been reported to have a direct or indirect regulatory relationship with AGO2. For instance, miR-1247 is associated with cancer prognosis, with its upregulation inhibiting the malignant progression of cancer [44,45]. Elevated expression of miR-142-5p can suppress PD-L1 expression in tumor cells, enhancing anti-tumor immune responses [46]. In contrast, increased levels of miR-9-3p were observed to promote cell proliferation and inhibit apoptosis in cases of medullary thyroid carcinoma [47]. Consistent with our findings, precursors miR-1247-3p and miR-142-5p were identified as protective factors for BC prognosis, while miR-9-3p was categorized as a risk factor (Fig. 2A). The interaction between miRNAs and m7G is still under investigation, and the insights gained from this study may contribute to the development and selection of BC treatments by identifying prognostic miRNAs targeting m7G modification.

This study categorized BC patients into risk groups to assess their prognosis. Individuals in the high-risk group exhibited a significantly lower survival rate compared to those in the low-risk category. The ROC curve illustrated that the model's AUC surpassed 0.7, signifying enhanced accuracy in predicting prognosis based on the risk signature. The construction of prognostic models incorporating relevant miRNA signatures has gained widespread recognition in clinical practice [48]. Subsequently, we developed a nomogram by combining risk scores and clinical features. The model demonstrated relatively high AUC values for predicting patient survival at 3, 5, and 10 years, confirming its robust predictive abilities. Furthermore, multivariate Cox regression analysis indicated that miRNA risk scores function as autonomous prognostic factors.

Recent years have witnessed increased attention devoted to immune infiltration as a prognostic and immunotherapy factor. To further explore the relationship between risk-scoring models and immune status, the prognostic signature was strongly associated with

immune diseases, immune cells, and immune-related pathways, as revealed by functional enrichment analysis. Analysis of distinct types of DEGs in the risk groups showed that these DEGs were predominantly associated with processes beyond the plasma membrane. They were primarily engaged in regulating immune receptor processes, leading to functions such as immune receptor activity and cytokine receptor binding (Fig. 4). These findings imply that this pathway might influence tumor migration and invasion, potentially reshaping the state of the TME.

Utilizing TCGA-BRCA data, we examined the relationship between immune cell subtypes and immune function through ssGSEA to elucidate the impact of m7G on tumor immunity. In contrast to the high-risk group, the low-risk group exhibited elevated levels of immune cell infiltration, including $CD8^+$ T cells, T helper cells, and tumor-infiltrating lymphocytes (TILs), except mast cells (Fig. 5D). The concept of tumors being either "immune-desert" or "immune-inflamed" implies that the absence of T cell infiltration within tumors significantly contributes to the restricted effectiveness of immunotherapies, such as immune checkpoint inhibitors (ICIs), in treating immune-desert tumors [49]. We noted a significant contrast in the TMEs between the two cohorts, with the low-risk group displaying a relatively heightened immune response compared to the higher-risk group. Although risk group-based analyses cannot identify hot tumors, they can predict relative efficacy. During our analysis of immune checkpoint gene expression, we predominantly observed heightened expressions of ICOSLG and CD276 in the high-risk cohort (Fig. 6A). Iwata et al. previously reported that ICOSLG promotes the proliferation of regulatory T cells and the production of IL-10, thereby promoting the advancement of glioblastoma [50]. Additionally, CD276 suppresses T cells and is usually associated with important functions in patients [51]. Furthermore, low-risk patients may also be more susceptible to *anti*-CTLA-4 and *anti*-PD-1 therapies (Fig. 6B). Indeed, the efficacy of *anti*-CTLA-4 and PD-1 has been demonstrated in the clinical treatment of BC and represents a new opportunity for treating BC [52]. It is, therefore, likely to be more effective to use ICIs in low-risk groups, according to this study.

An analysis of drug sensitivity also indicated that the low-risk groups might exhibit increased susceptibility to ribociclib, vincristine, gemcitabine, epirubicin, and mitoxantrone. In high-risk patients, lapatinib conferred a more substantial benefit. The RIBECCA trial demonstrated that the combination of ribociclib plus letrozole decreased regulatory T cell and immunosuppressive cytokine signaling in peripheral blood, activating adaptive immune responses in BC patients [53]. Another study showed that lapatinib plus anthracyclines could enhance tumor infiltration by T cells secreting IFN-γ, playing an important role in building an antitumor immune response [54]. These findings may help develop clinical strategies for combining chemotherapeutic and immunotherapeutic drugs to mitigate drug resistance. Hence, we posit that the m7G-related miRNA signature can provide valuable insights for tailoring personalized treatment approaches for BC patients.

Nevertheless, there are certain constraints within this study. For instance, the data utilized in this research are derived from publicly available databases, and our internal validation relies solely on TCGA data, potentially introducing some degree of selection bias into the analysis results. A follow-up large, multi-center, prospective study is needed to confirm our results further. In addition, the accuracy of the m7G-related miRNA scoring model in predicting drug efficacy also needs to be confirmed by clinical trials.

5. Conclusion

To summarize, this study thoroughly analyzed m7G-related miRNAs, providing insights into their regulatory mechanisms within the tumor microenvironment, pathological features, and prognosis in BC patients. The results demonstrate the clinical value of m7G-related miRNAs and establish and validate a nomogram. By predicting chemotherapy and immunotherapy response, m7G-related miRNA signatures may also guide individualized BC treatment.

Data availability statement

Data included in article/supp. material/referenced in article.

Ethics statement

All data used in the study was obtained from public databases, hence, ethics approval and informed consent were not required.

Consent to participate

Not applicable.

Consent for publication

The authors declare that they agree to submit the article for publication.

Funding

This work was supported by funds from the Basic and Applied Basic Research Foundation of Guangdong Province (2023A1515110933, Danian Dai), the Science and Technology Program of Guangzhou (2023A04J0527, Danian Dai; 202201011427, Bo Chen), the Natural Science Foundation of Guangdong Province, China (2022A1515011599, Bo Chen), the Excellent Young Talent Program of Guangdong Provincial People's Hospital (KY012021190, Bo Chen), the National Natural Science Foundation of China

(82272998 Bo Chen), the High-level Hospital Construction Project (DFJH201921, Bo Chen). The funding agencies had no role in the design of the study, the collection, analysis, and interpretation of data, or the writing of the manuscript.

CRediT authorship contribution statement

Danian Dai: Writing – review & editing, Writing – original draft, Funding acquisition, Formal analysis, Data curation, Conceptualization. **Hongkai Zhuang:** Writing – review & editing, Visualization, Methodology, Investigation, Formal analysis. **Mao Shu:** Writing – review & editing, Visualization, Supervision, Resources, Formal analysis. **Lezi Chen:** Resources, Methodology, Investigation, Formal analysis. **Chen Long:** Visualization, Supervision, Resources, Methodology, Investigation. **Hongmei Wu:** Writing – review & editing, Writing – original draft, Supervision, Investigation, Funding acquisition, Formal analysis. **Bo Chen:** Writing – review & editing, Visualization, Validation, Supervision, Investigation, Funding acquisition, Conceptualization.

Declaration of competing interest

The authors declare that they have no known competing financial interests or personal relationships that could have appeared to influence the work reported in this paper.

Appendix A. Supplementary data

Supplementary data to this article can be found online at https://doi.org/10.1016/j.heliyon.2024.e29326.

References

[1] C. Xia, X. Dong, H. Li, M. Cao, D. Sun, S. He, F. Yang, X. Yan, S. Zhang, N. Li, W. Chen, Cancer statistics in China and United States, 2022: profiles, trends, and determinants, Chin. Med. J. 135 (2022) 584–590, https://doi.org/10.1097/CM9.0000000000002108.
[2] D. Dai, H. Wu, H. Zhuang, R. Chen, C. Long, B. Chen, Genetic and clinical landscape of ER +/PR- breast cancer in China, BMC Cancer 23 (2023) 1189, https://doi.org/10.1186/s12885-023-11643-2.
[3] N. Bilani, E.C. Zabor, L. Elson, E.B. Elimimian, Z. Nahleh, Breast cancer in the United States: a cross-sectional overview, J. Cancer Epidemiol. 2020 (2020) 6387378, https://doi.org/10.1155/2020/6387378.
[4] L.A. Emens, Breast cancer immunotherapy: facts and hopes, Clin. Cancer Res. 24 (2018) 511–520, https://doi.org/10.1158/1078-0432.CCR-16-3001.
[5] D. Peng, I. Kryczek, N. Nagarsheth, L. Zhao, S. Wei, W. Wang, Y. Sun, E. Zhao, L. Vatan, W. Szeliga, J. Kotarski, R. Tarkowski, Y. Dou, K. Cho, S. Hensley-Alford, A. Munkarah, R. Liu, W. Zou, Epigenetic silencing of TH1-type chemokines shapes tumour immunity and immunotherapy, Nature 527 (2015) 249–253, https://doi.org/10.1038/nature15520.
[6] Y. Zou, F. Ye, Y. Kong, X. Hu, X. Deng, J. Xie, C. Song, X. Ou, S. Wu, L. Wu, Y. Xie, W. Tian, Y. Tang, C.-W. Wong, Z.-S. Chen, X. Xie, H. Tang, The single-cell landscape of intratumoral heterogeneity and the immunosuppressive microenvironment in liver and brain metastases of breast cancer, Adv. Sci. 10 (2023) e2203699, https://doi.org/10.1002/advs.202203699.
[7] J. Xie, Y. Zou, F. Ye, W. Zhao, X. Xie, X. Ou, X. Xie, W. Wei, A novel platelet-related gene signature for predicting the prognosis of triple-negative breast cancer, Front. Cell Dev. Biol. 9 (2021) 795600, https://doi.org/10.3389/fcell.2021.795600.
[8] J. Xie, J. Zhang, W. Tian, Y. Zou, Y. Tang, S. Zheng, C.-W. Wong, X. Deng, S. Wu, J. Chen, Y. Mo, X. Xie, The pan-cancer multi-omics landscape of FOXO family relevant to clinical outcome and drug resistance, Int. J. Mol. Sci. 23 (2022) 15647, https://doi.org/10.3390/ijms232415647.
[9] Y. Tang, Y. Wang, M.F. Kiani, B. Wang, Classification, treatment strategy, and associated drug resistance in breast cancer, Clin. Breast Cancer 16 (2016) 335–343, https://doi.org/10.1016/j.clbc.2016.05.012.
[10] T. Carell, C. Brandmayr, A. Hienzsch, M. Müller, D. Pearson, V. Reiter, I. Thoma, P. Thumbs, M. Wagner, Structure and function of noncanonical nucleobases, Angew Chem. Int. Ed. Engl. 51 (2012) 7110–7131, https://doi.org/10.1002/anie.201201193.
[11] M.A. Machnicka, K. Milanowska, O. Osman Oglou, E. Purta, M. Kurkowska, A. Olchowik, W. Januszewski, S. Kalinowski, S. Dunin-Horkawicz, K.M. Rother, M. Helm, J.M. Bujnicki, H. Grosjean, MODOMICS: a database of RNA modification pathways–2013 update, Nucleic Acids Res. 41 (2013) D262–D267, https://doi.org/10.1093/nar/gks1007.
[12] Y. Furuichi, Discovery of m(7)G-cap in eukaryotic mRNAs, Proc. Jpn. Acad. Ser. B Phys. Biol. Sci. 91 (2015) 394–409, https://doi.org/10.2183/pjab.91.394.
[13] C. Tomikawa, 7-Methylguanosine modifications in transfer RNA (tRNA), Int. J. Mol. Sci. 19 (2018) 4080, https://doi.org/10.3390/ijms19124080.
[14] Y. Luo, Y. Yao, P. Wu, X. Zi, N. Sun, J. He, The potential role of N7-methylguanosine (m7G) in cancer, J. Hematol. Oncol. 15 (2022) 63, https://doi.org/10.1186/s13045-022-01285-5.
[15] E.A. Orellana, Q. Liu, E. Yankova, M. Pirouz, E. De Braekeleer, W. Zhang, J. Lim, D. Aspris, E. Sendinc, D.A. Garyfallos, M. Gu, R. Ali, A. Gutierrez, S. Mikutis, G. J.L. Bernardes, E.S. Fischer, A. Bradley, G.S. Vassiliou, F.J. Slack, K. Tzelepis, R.I. Gregory, METTL1-mediated m7G modification of Arg-TCT tRNA drives oncogenic transformation, Mol. Cell. 81 (2021) 3323–3338.e14, https://doi.org/10.1016/j.molcel.2021.06.031.
[16] J. Chen, K. Li, J. Chen, X. Wang, R. Ling, M. Cheng, Z. Chen, F. Chen, Q. He, S. Li, C. Zhang, Y. Jiang, Q. Chen, A. Wang, D. Chen, Aberrant translation regulated by METTL1/WDR4-mediated tRNA N7-methylguanosine modification drives head and neck squamous cell carcinoma progression, Cancer Commun. 42 (2022) 223–244, https://doi.org/10.1002/cac2.12273.
[17] G. Di Leva, C.M. Croce, miRNA profiling of cancer, Curr. Opin. Genet. Dev. 23 (2013) 3–11, https://doi.org/10.1016/j.gde.2013.01.004.
[18] L. Pandolfini, I. Barbieri, A.J. Bannister, A. Hendrick, B. Andrews, N. Webster, P. Murat, P. Mach, R. Brandi, S.C. Robson, V. Migliori, A. Alendar, M. d'Onofrio, S. Balasubramanian, T. Kouzarides, METTL1 promotes let-7 MicroRNA processing via m7G methylation, Mol. Cell. 74 (2019) 1278–1290.e9, https://doi.org/10.1016/j.molcel.2019.03.040.
[19] H. Xie, M. Wang, H. Yu, H. Wang, L. Ding, R. Wang, W. Luo, Z. Lu, Q. Zheng, L. Ren, Z. Zhou, W. Su, L. Xia, G. Li, METTL1 drives tumor progression of bladder cancer via degrading ATF3 mRNA in an m7G-modified miR-760-dependent manner, Cell Death Dis. 8 (2022) 458, https://doi.org/10.1038/s41420-022-01236-6.
[20] W. Mei, X. Jia, S. Xin, X. Liu, L. Jin, X. Sun, J.-X. Zhang, B. Zhang, G. Yang, P. Chen, L. Ye, A N7-methylguanine-related gene signature applicable for the prognosis and microenvironment of prostate cancer, JAMA Oncol. 2022 (2022) 8604216, https://doi.org/10.1155/2022/8604216.
[21] J. Ming, C. Wang, N7-Methylguanosine-Related lncRNAs: integrated analysis associated with prognosis and progression in clear cell renal cell carcinoma, Front. Genet. 13 (2022) 871899, https://doi.org/10.3389/fgene.2022.871899.

[22] K. Yoshihara, M. Shahmoradgoli, E. Martínez, R. Vegesna, H. Kim, W. Torres-Garcia, V. Treviño, H. Shen, P.W. Laird, D.A. Levine, S.L. Carter, G. Getz, K. Stemke-Hale, G.B. Mills, R.G.W. Verhaak, Inferring tumour purity and stromal and immune cell admixture from expression data, Nat. Commun. 4 (2013) 2612, https://doi.org/10.1038/ncomms3612.
[23] M. Carlson, , et al.org Hs eg db, Genome wide annotation for Human, R package version 3 (2) (2019) 3.
[24] G. Yu, L.-G. Wang, Y. Han, Q.-Y. He, clusterProfiler: an R package for comparing biological themes among gene clusters, OMICS 16 (2012) 284–287, https://doi.org/10.1089/omi.2011.0118.
[25] E.M. Van Allen, D. Miao, B. Schilling, S.A. Shukla, C. Blank, L. Zimmer, A. Sucker, U. Hillen, M.H.G. Foppen, S.M. Goldinger, J. Utikal, J.C. Hassel, B. Weide, K. C. Kaehler, C. Loquai, P. Mohr, R. Gutzmer, R. Dummer, S. Gabriel, C.J. Wu, D. Schadendorf, L.A. Garraway, Genomic correlates of response to CTLA-4 blockade in metastatic melanoma, Science 350 (2015) 207–211, https://doi.org/10.1126/science.aad0095.
[26] W. Hugo, J.M. Zaretsky, L. Sun, C. Song, B.H. Moreno, S. Hu-Lieskovan, B. Berent-Maoz, J. Pang, B. Chmielowski, G. Cherry, E. Seja, S. Lomeli, X. Kong, M. C. Kelley, J.A. Sosman, D.B. Johnson, A. Ribas, R.S. Lo, Genomic and transcriptomic features of response to anti-PD-1 therapy in metastatic melanoma, Cell 168 (2017) 542, https://doi.org/10.1016/j.cell.2017.01.010.
[27] D. Maeser, R.F. Gruener, R.S. Huang, oncoPredict: an R package for predicting in vivo or cancer patient drug response and biomarkers from cell line screening data, Briefings Bioinf. 22 (2021), https://doi.org/10.1093/bib/bbab260 bbab260.
[28] W. Shen, Z. Song, X. Zhong, M. Huang, D. Shen, P. Gao, X. Qian, M. Wang, X. He, T. Wang, S. Li, X. Song, Sangerbox: a comprehensive, interaction-friendly clinical bioinformatics analysis platform, iMeta 1 (2022) e36, https://doi.org/10.1002/imt2.36.
[29] J. Jovanovic, J.A. Rønneberg, J. Tost, V. Kristensen, The epigenetics of breast cancer, Mol. Oncol. 4 (2010) 242–254, https://doi.org/10.1016/j.molonc.2010.04.002.
[30] L. de la Cruz-Merino, A. Barco-Sánchez, F. Henao Carrasco, E. Nogales Fernández, A. Vallejo Benítez, J. Brugal Molina, A. Martínez Peinado, A. Grueso López, M. Ruiz Borrego, M. Codes Manuel de Villena, V. Sánchez-Margalet, A. Nieto-García, E. Alba Conejo, N. Casares Lagar, J. Ibáñez Martínez, New insights into the role of the immune microenvironment in breast carcinoma, Clin. Dev. Immunol. 2013 (2013) 785317, https://doi.org/10.1155/2013/785317.
[31] N.A. Giraldo, R. Sanchez-Salas, J.D. Peske, Y. Vano, E. Becht, F. Petitprez, P. Validire, A. Ingels, X. Cathelineau, W.H. Fridman, C. Sautès-Fridman, The clinical role of the TME in solid cancer, Br. J. Cancer 120 (2019) 45–53, https://doi.org/10.1038/s41416-018-0327-z.
[32] H. Liu, X. Zeng, X. Ren, Y. Zhang, M. Huang, L. Tan, Z. Dai, J. Lai, W. Xie, Z. Chen, S. Peng, L. Xu, S. Chen, S. Shen, M. Kuang, S. Lin, Targeting tumour-intrinsic N7-methylguanosine tRNA modification inhibits MDSC recruitment and improves anti-PD-1 efficacy, Gut 72 (2023) 1555–1567, https://doi.org/10.1136/gutjnl-2022-327230.
[33] K.B. Reddy, MicroRNA (miRNA) in cancer, Cancer Cell Int. 15 (2015) 38, https://doi.org/10.1186/s12935-015-0185-1.
[34] M. Kiriakidou, G.S. Tan, S. Lamprinaki, M. De Planell-Saguer, P.T. Nelson, Z. Mourelatos, An mRNA m7G cap binding-like motif within human Ago2 represses translation, Cell 129 (2007) 1141–1151, https://doi.org/10.1016/j.cell.2007.05.016.
[35] Y. Lai, Y. Chen, Y. Lin, L. Ye, Down-regulation of LncRNA CCAT1 enhances radiosensitivity via regulating miR-148b in breast cancer, Cell Biol. Int. 42 (2018) 227–236, https://doi.org/10.1002/cbin.10890.
[36] H. Liu, D. Chen, J. Bi, J. Han, M. Yang, W. Dong, T. Lin, J. Huang, Circular RNA circUBXN7 represses cell growth and invasion by sponging miR-1247-3p to enhance B4GALT3 expression in bladder cancer, Aging (Albany NY) 10 (2018) 2606–2623, https://doi.org/10.18632/aging.101573.
[37] Y. Jia, Y. Duan, T. Liu, X. Wang, W. Lv, M. Wang, J. Wang, L. Liu, LncRNA TTN-AS1 promotes migration, invasion, and epithelial mesenchymal transition of lung adenocarcinoma via sponging miR-142-5p to regulate CDK5, Cell Death Dis. 10 (2019) 573, https://doi.org/10.1038/s41419-019-1811-y.
[38] P. Wu, J. Cai, Q. Chen, B. Han, X. Meng, Y. Li, Z. Li, R. Wang, L. Lin, C. Duan, C. Kang, C. Jiang, Lnc-TALC promotes O6-methylguanine-DNA methyltransferase expression via regulating the c-Met pathway by competitively binding with miR-20b-3p, Nat. Commun. 10 (2019) 2045, https://doi.org/10.1038/s41467-019-10025-2.
[39] X. Zhao, Q. Zhong, X. Cheng, S. Wang, R. Wu, X. Leng, L. Shao, miR-449c-5p availability is antagonized by circ-NOTCH1 for MYC-induced NOTCH1 upregulation as well as tumor metastasis and stemness in gastric cancer, J. Cell. Biochem. 121 (2020) 4052–4063, https://doi.org/10.1002/jcb.29575.
[40] Z. Wu, Q. Gong, Y. Yu, J. Zhu, W. Li, Knockdown of circ-ABCB10 promotes sensitivity of lung cancer cells to cisplatin via miR-556-3p/AK4 axis, BMC Pulm. Med. 20 (2020) 10, https://doi.org/10.1186/s12890-019-1035-z.
[41] L. Wang, J. Yi, L.-Y. Lu, Y.-Y. Zhang, L. Wang, G.-S. Hu, Y.-C. Liu, J.-C. Ding, H.-F. Shen, F.-Q. Zhao, H.-H. Huang, W. Liu, Estrogen-induced circRNA, circPGR, functions as a ceRNA to promote estrogen receptor-positive breast cancer cell growth by regulating cell cycle-related genes, Theranostics 11 (2021) 1732–1752, https://doi.org/10.7150/thno.45302.
[42] X. Zhou, H. Ye, X. Wang, J. Tu, J. Lv, MiR-375 and miR-5691 exert anti-fibroproliferative effects on hypertrophic scar fibroblasts by suppressing thrombospondin 1 expression, Dermatol. Sin. 40 (2022) 34, https://doi.org/10.4103/ds.ds_13_22.
[43] Y. Shi, C.-F. Sun, W.-H. Ge, Y.-P. Du, N.-B. Hu, Circular RNA VMA21 ameliorates sepsis-associated acute kidney injury by regulating miR-9-3p/SMG1/inflammation axis and oxidative stress, J. Cell Mol. Med. 24 (2020) 11397–11408, https://doi.org/10.1111/jcmm.15741.
[44] M.L. Taddei, L. Cavallini, M. Ramazzotti, G. Comito, L. Pietrovito, A. Morandi, E. Giannoni, G. Raugei, P. Chiarugi, Stromal-induced downregulation of miR-1247 promotes prostate cancer malignancy, J. Cell. Physiol. 234 (2019) 8274–8285, https://doi.org/10.1002/jcp.27679.
[45] J.M. Yi, E.-J. Kang, H.-M. Kwon, J.-H. Bae, K. Kang, N. Ahuja, K. Yang, Epigenetically altered miR-1247 functions as a tumor suppressor in pancreatic cancer, Oncotarget 8 (2017) 26600–26612, https://doi.org/10.18632/oncotarget.15722.
[46] L. Jia, Q. Xi, H. Wang, Z. Zhang, H. Liu, Y. Cheng, X. Guo, J. Zhang, Q. Zhang, L. Zhang, Z. Xue, Y. Li, Y. Da, P. Zhao, R. Zhang, miR-142-5p regulates tumor cell PD-L1 expression and enhances anti-tumor immunity, Biochem. Biophys. Res. Commun. 488 (2017) 425–431, https://doi.org/10.1016/j.bbrc.2017.05.074.
[47] Y. Chen, S. Zhang, R. Zhao, Q. Zhao, T. Zhang, Upregulated miR-9-3p promotes cell growth and inhibits apoptosis in medullary thyroid carcinoma by targeting BLCAP, Oncol. Res. 25 (2017) 1215–1222, https://doi.org/10.3727/096504016X14791715355957.
[48] Z. Zheng, Y. Wen, K. Nie, S. Tang, X. Chen, S. Lan, J. Pan, K. Jiang, X. Jiang, P. Liu, Y. Yan, F. Liu, Y. Liu, P. Li, Construction of a 13-microRNA-based signature and prognostic nomogram for predicting overall survival in patients with hepatocellular carcinoma, Hepatol. Res. 50 (2020) 1151–1163, https://doi.org/10.1111/hepr.13538.
[49] Y.-T. Liu, Z.-J. Sun, Turning cold tumors into hot tumors by improving T-cell infiltration, Theranostics 11 (2021) 5365–5386, https://doi.org/10.7150/thno.58390.
[50] R. Iwata, J. Hyoung Lee, M. Hayashi, U. Dianzani, K. Ofune, M. Maruyama, S. Oe, T. Ito, T. Hashiba, K. Yoshimura, M. Nonaka, Y. Nakano, L. Norian, I. Nakano, A. Asai, ICOSLG-mediated regulatory T-cell expansion and IL-10 production promote progression of glioblastoma, Neuro Oncol. 22 (2020) 333–344, https://doi.org/10.1093/neuonc/noz204.
[51] E. Picarda, K.C. Ohaegbulam, X. Zang, Molecular pathways: targeting B7-H3 (CD276) for human cancer immunotherapy, Clin. Cancer Res. 22 (2016) 3425–3431, https://doi.org/10.1158/1078-0432.CCR-15-2428.
[52] S. Adams, M. Othus, S.P. Patel, K.D. Miller, R. Chugh, S.M. Schuetze, M.D. Chamberlin, B.J. Haley, A.M.V. Storniolo, M.P. Reddy, S.A. Anderson, C. T. Zimmerman, A.P. O'Dea, H.R. Mirshahidi, J.R. Ahnert, F.J. Brescia, O. Hahn, J.M. Raymond, D.D. Biggs, R.M. Connolly, E. Sharon, L.A. Korde, R.J. Gray, E. Mayerson, M. Plets, C.D. Blanke, Y.K. Chae, R. Kurzrock, A multicenter phase II trial of ipilimumab and nivolumab in unresectable or metastatic metaplastic breast cancer: cohort 36 of dual anti-CTLA-4 and anti-PD-1 blockade in rare tumors (DART, SWOG S1609), Clin. Cancer Res. 28 (2022) 271–278, https://doi.org/10.1158/1078-0432.CCR-21-2182.
[53] C.A. Peuker, S. Yaghobramzi, C. Grunert, L. Keilholz, E. Gjerga, S. Hennig, S. Schaper, I.-K. Na, U. Keller, S. Brucker, T. Decker, P. Fasching, T. Fehm, W. Janni, S. Kümmel, A. Schneeweiss, M. Schuler, D. Lüftner, A. Busse, Treatment with ribociclib shows favourable immunomodulatory effects in patients with hormone receptor-positive breast cancer-findings from the RIBECCA trial, Eur. J. Cancer 162 (2022) 45–55, https://doi.org/10.1016/j.ejca.2021.11.025.
[54] L. Hannesdóttir, P. Tymoszuk, N. Parajuli, M.-H. Wasmer, S. Philipp, N. Daschil, S. Datta, J.-B. Koller, C.H. Tripp, P. Stoitzner, E. Müller-Holzner, G.J. Wiegers, V. Sexl, A. Villunger, W. Doppler, Lapatinib and doxorubicin enhance the Stat1-dependent antitumor immune response, Eur. J. Immunol. 43 (2013) 2718–2729, https://doi.org/10.1002/eji.201242505.